Real-Time Planner for Multi-segment Continuum Manipulator in Dynamic Environments*

Ahmad Ataka, Peng Qi, Hongbin Liu, and Kaspar Althoefer

Abstract— **In this paper, a potential-field-based real-time path planning algorithm for a multi-segment continuum manipulator is proposed. This planner is employed to enable a continuum-style manipulator to move autonomously in dynamic environments in real-time. The classic potential field method is modified to make it applicable for a kinematics model based on the constant-curvature assumption. The contribution of this paper lies in the design of a novel potential field in the actuator space satisfying the mechanical constraints of the manipulator. The planning algorithm is tested and validated in real-time simulation for a 3 segments continuum manipulator. Preliminary tests for a tendon-driven single-segment continuum manipulator prototype confirm the performance of the proposed planner.**

I. INTRODUCTION

Nowadays, continuum manipulators, such as those inspired by the octopus [1] or the snake [2] have gained much popularity in the field of robotics due to their flexibility and dexterity. In recent years, researchers tried to implement continuum manipulators in application areas where a high risk may be posed if tasks were handled by rigid-link manipulators - examples include surgery and other medical-related areas. However, although the robot's ability to bend at any point along its backbone makes it particularly safe to be used in the medical field, automation is still needed to further improve safety and ensure high maneuverability.

In the last decade, various continuum robot structures have been reported by several researchers [3]- [5]; studies on the kinematic modelling, Jacobian, dynamic modelling, and control of continuum manipulator start to appear as reported in [6]. However, research on continuum manipulator navigation is still in its infancy and clearly a challenging problem, largely because of the complexity of the manipulator's model.

One recent study on path planning for continuum manipulator's which uses a simple and fast geometrical inverse kinematic solution of a constant-curvature steerable needle was reported in [7]. However, this method cannot be used to deal with obstacles dynamically changing their position, because it assumes a static and well-defined environment. Most works which use optimization-based planning [8]- [10] and sampling-based planning [11]- [13] also suffer from the same drawback.

Studies on path planning for real-time applications have been reported in recent years. Xiao proposed a real-time adaptive motion planning approach for OctArm manipulator in dynamic environments [14]. However, the algorithm is limited to the planar case and does not produce solutions in actuator space limiting its applicability. Chen proposed inverse-Jacobian-based planning which provides solutions in actuator space [15], but it is specifically designed to guide the movement of manipulator inside a tubular environment. Another research work reported by Godage [16] exploits the null space of a highly redundant multi-segment continuum manipulator model. However, its mathematical calculation is costly due to the fact that it involves successive matrix multiplication. Besides, the hard-limiting function used to model the mechanical constraint influences the smoothness of manipulator's movement when the tendons are close to their limits.

One of the popular works in this area is the artificial potential field method [17]. It is largely used for robots such as mobile robots and rigid manipulators, especially because of its simplicity and straightforward way of implementing. Some researchers have applied potential field method to continuum robots, such as steerable needle [18]. Although the algorithm does not ensure global convergence, a global map of the environment is not needed and, hence, it can be used in dynamic and unknown environments, thus, makes it suitable for real-time applications.

In this work, we propose potential-field-based real-time path planning for a multi-segment continuum manipulator. The planner presented in [17] is modified to make it applicable to a constant-curvature kinematic model. We also propose a novel potential field for the actuator space to satisfy the mechanical constraints of the manipulator. The novel potential field in actuator space also improves the standard hard-limiting function usually employed to satisfy mechanical constraints due to the fact that the proposed method does not disturb the smoothness of the manipulator motion. The planning algorithm is tested and validated in a real-time simulation on a 3 segment continuum manipulator. Conducting tests on a real tendon-driven single-segment continuum manipulator prototype (previously described in [19]) confirms the performance of the proposed planner in a real-world application.

*The work described in this paper is partially supported by the STIFF-FLOP project grant from the European Communities Seventh Framework Programme under grant agreement 287728, the Four By Three grant from the European Framework Programme for Research and Innovation Horizon 2020 under grant agreement no 637095, and the Indonesia Endowment Fund for Education, Ministry of Finance Republic of Indonesia.

Ahmad Ataka, Peng Qi, Hongbin Liu, and Kaspar Althoefer is with The Centre for Robotics Research (CoRe), Department of Informatics, Kings College London, London WC2R 2LS, United Kingdom. Corresponding author e-mail: ahmad_ataka_awwalur.rizqi@kcl.ac.uk

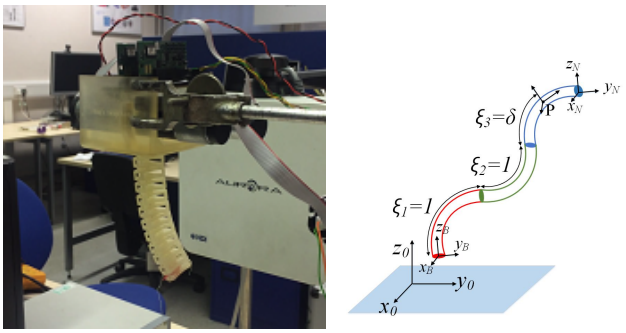

(a) (b)

Fig. 1. (a) The single-segment tendon-driven continuum manipulator used in the experiment. (b) Three segments continuum manipulator with movable base. A point P located at δs_3 along the backbone of the third segment can be expressed with the help of the scalar coefficient vector $\xi = [1 \quad 1 \quad \delta]^T$

II. CONTINUUM MANIPULATOR MODEL

In this section, the constant-curvature kinematic model is described. We assume that every segment of the manipulator acts like the arc of a circle with a constant radius of curvature along each individual robot segment. Hence, assuming the manipulator moves in $\mathbb{R}^3$, each segment can be parameterized by three configuration space variables $\mathbf{k}_i = \begin{bmatrix}\kappa_i & \phi_i & s_i\end{bmatrix}^T$. These variables represent the curvature (κ_i), rotational deflection angle (ϕ_i), and arc length (s_i) of a segment-i. The homogeneous transformation matrix describing the tip pose of segment i with respect to the base, ${}^{i}_{i-1}\mathbf{T}(\mathbf{k}_i) \in SE(3)$, can be expressed as function of $\mathbf{k}_i$ as given in [6].

We assume the base of the continuum manipulator is movable with 6 degrees of freedom, such that the pose of the end effector with respect to the world frame for N segments manipulator can be expressed as follows

$$ {}^{N}_{0}\mathbf{T}(\mathbf{k}) = \mathbf{T}_B \prod_{i=1}^{N} {}^{i}_{i-1}\mathbf{T}(\mathbf{k}_i) \tag{1} $$

where $\mathbf{k} = \begin{bmatrix}\mathbf{k}_1 & \mathbf{k}_2 & \dots & \mathbf{k}_N\end{bmatrix}^T$ and $\mathbf{T}_B \in SE(3)$ represents the standard homogeneous transformation matrix of the frame attached to the base with 6 degrees of freedom.

Further mapping is needed to construct the relation between the previous configuration space variables $\mathbf{k}$ to the actuator space variables $\mathbf{q}$. For a tendon-driven continuum manipulator, the actuator space variables of segment-i can be expressed as $\mathbf{q}_i = \begin{bmatrix}l_{i1} & l_{i2} & l_{i3}\end{bmatrix}^T$ where l_{ij} represents the length of tendon-j in segment-i. The overall actuator space variables for N segments manipulator can then be written as $\mathbf{q} = \begin{bmatrix}\mathbf{q}_0 & \mathbf{q}_1 & \dots & \mathbf{q}_N\end{bmatrix}^T$ where $\mathbf{q}_0 \in \mathbf{R}^6$ represents the base's position and orientation. The configuration space variables of segment-i, $\mathbf{k}_i$, can be expressed as function of manipulator's cross-section radius d and tendon length in segment-i, $\mathbf{q}_i$, as expressed in [6].

The scalar coefficient vector, defined in [16], is used to express the pose of any point along the backbone of the manipulator. A scalar $\xi_i \in [0,1]$ is assigned to each segment to specify the point along the segment, from the base ($\xi_i = 0$) to the tip ($\xi_i = 1$) of segment-i. The set of scalars of all segments are then formed into a vector, $\xi = \begin{bmatrix}\xi_1 & \xi_2 & \dots & \xi_N\end{bmatrix}^T$. The value of the vector is defined as $\xi = \{\xi_r = 1 : \forall r < i, \xi_i, \xi_r = 0 : \forall r > i\}$. An example is presented in Figure 1b.

Hence, the complete forward kinematic relation can be expressed as follows

$$ {}^{N}_{0}\mathbf{T}(\mathbf{q},\xi) = \begin{bmatrix}\mathbf{R}(\mathbf{q},\xi) & \mathbf{x}(\mathbf{q},\xi) \\ \mathbf{0}_{1\times 3} & 1\end{bmatrix} \tag{2} $$

where $\mathbf{R}(\mathbf{q},\xi) \in SO(3)$ denotes the rotation matrix and $\mathbf{x}(\mathbf{q},\xi) \in \mathbb{R}^3$ denotes the position vector of the point along the body of manipulator. A Jacobian, defined as $\mathbf{J}(\mathbf{q},\xi) = \frac{\partial \mathbf{x}(\mathbf{q},\xi)}{\partial \mathbf{q}} \in \mathbb{R}^{3\times(3N+6)}$, relates the velocity vector as follows

$$ \dot{\mathbf{x}}(\mathbf{q},\xi) = \mathbf{J}(\mathbf{q},\xi)\dot{\mathbf{q}} \Leftrightarrow \dot{\mathbf{q}} = \mathbf{J}(\mathbf{q},\xi)^{-1}\dot{\mathbf{x}}(\mathbf{q},\xi). \tag{3} $$

III. POTENTIAL-FIELD-BASED PATH PLANNING

A. Classic Potential Field

The planning algorithm, used in this paper, is based on [17]. The manipulator in general moves in configuration space (C-Space) filled employing an artificial potential field $U(\mathbf{q})$ which attracts the manipulator to the desired target configuration, whilst repelling it from configurations where the manipulator would touch obstacles (C-obstacle region). The generalized force which guides the movement of the manipulator can be expressed as

$$ \mathbf{F}(\mathbf{q}) = -\nabla U(\mathbf{q}). \tag{4} $$

The attractive parabolic potential function for a desired configuration $\mathbf{q}_d$ can be expressed as

$$ U_d(\mathbf{q}) = \frac{1}{2}k(\mathbf{q}-\mathbf{q}_d)^T(\mathbf{q}-\mathbf{q}_d), \tag{5} $$

where k is constant gain. The repulsive potential produced by obstacles $\mathscr{O}$ can be expressed as follows

$$ U_{\mathscr{O}}(\mathbf{q}) = \begin{cases} \frac{1}{2}\eta(\frac{1}{\rho}-\frac{1}{\rho_0})^2 & \text{if } \rho < \rho_0 \\ 0 & \text{if } \rho > \rho_0 \end{cases} \tag{6} $$

where $\rho = \sqrt{(\mathbf{q}-\mathbf{q}_{\mathscr{O}})^T(\mathbf{q}-\mathbf{q}_{\mathscr{O}})}$ is the closest Euclidean distance between the manipulator's configuration and the C-obstacle region in C-Space, η is positive constant, and ρ_0 is the limit distance of the potential influence.

The resulting potential is given by a linear combination of attractive and repulsive potentials from all obstacles. An illustration is shown in Figure 2a.

B. Modified Potential Field

The potential field can be easily applied in a C-Space. However, to construct the C-Space for N segments continuum manipulator with a movable base, which has $3N+6$ degrees of freedom, is not feasible especially for real-time planning purpose. Hence, we can use the same approach applied to rigid-link manipulator [17] or steerable-needle [18] by producing a potential function $U(\mathbf{x})$ in the workspace of manipulator.

Since we will use the kinematic model of a continuum manipulator, a generalized force $\mathbf{F}$ in the classic algorithm is considered as the velocity of the manipulator $\dot{\mathbf{x}}$. Hence,

the spatial velocity $\dot{\mathbf{x}}(\mathbf{x})$, derived from the gradient of the potential $U(\mathbf{x})$, is then mapped to an actuator space velocity $\dot{\mathbf{q}}(\mathbf{q})$ by an inverse Jacobian relation in (3).

The attractive velocity in workspace is given by

$$\dot{\mathbf{x}}_{\mathbf{x}_d}(\mathbf{x}) = -\nabla U_d(\mathbf{x}) = -k(\mathbf{x}-\mathbf{x}_d), \tag{7}$$

where $\mathbf{x}_d$ represents the desired end effector's position in the workspace. The repulsive velocity can be calculated as follows

$$\dot{\mathbf{x}}_{\mathscr{O}_b}(\mathbf{x}) = -\nabla U_{\mathscr{O}_b}(\mathbf{x}) = \begin{cases} \eta(\frac{1}{\rho_b}-\frac{1}{\rho_0})\frac{1}{\rho_b^2}\frac{\partial \rho_b}{\partial \mathbf{x}} & \text{if } \rho_b < \rho_0 \\ 0 & \text{if } \rho_b > \rho_0 \end{cases}. \tag{8}$$

Here, $\rho_b = \sqrt{(\mathbf{x}-\mathbf{x}_{\mathscr{O}_b})^T(\mathbf{x}-\mathbf{x}_{\mathscr{O}_b})}$ represents the closest Euclidean distance between the manipulator's end effector's position and the obstacle-b in workspace.

Applying the repulsive velocity to the end effector alone is not sufficient to ensure that the whole body of the manipulator will avoid the obstacles. An approach given in [17] applied the repulsive force on each *point subjected to potential* (PSP) along the body of the manipulator. The higher the number of PSPs along the body of the manipulator, the more collisions with obstacles are avoided.

Finally, we transform each spatial velocity, applied in the end effector and PSPs, to the corresponding actuator space velocity. For m number of PSP and n number of point obstacles in the vicinity of the robot, the total velocity in the actuator space can be expressed as follows

$$\dot{\mathbf{q}}(\mathbf{q}) = \mathbf{J}_e(\mathbf{q})^+ \dot{\mathbf{x}}_{\mathbf{x}_d}(\mathbf{x}) + \sum_{a=1}^{m}\sum_{b=1}^{n} \mathbf{J}_a(\mathbf{q})^+ \dot{\mathbf{x}}_{\mathscr{O}_b}(\mathbf{x}) \tag{9}$$

where $\mathbf{J}_e$ and $\mathbf{J}_a$ stands for the Jacobian of the end effector's and the Jacobian of the PSP-a respectively, with the elements value of scalar coefficient vector ξ depending on the position of the PSP along the backbone of the manipulator. The $(^+)$ operation represents the pseudo-inverse matrix operation based on [20] defined as

$$\mathbf{J}^+ = \mathbf{J}^T(\mathbf{J}\mathbf{J}^T)^{-1}. \tag{10}$$

C. Mechanical Constraint Avoidance

The novelty of this work compared to previous works is the utilization of a novel potential field in the actuator space to guide the continuum manipulator to avoid limits due to the mechanical design of the manipulator. The continuum manipulator used in this paper is assumed to have mechanical constraint in its tendon length, namely it can only be extended or shortened with ratio ζ. In other words, the length of each tendon is inside the region $(1-\zeta)L < l_{ij} < (1+\zeta)L$ where L stands for the normal length without contraction or elongation.

Rather than applying the repulsive potential for these limits, which will disturb the movement's smoothness when the tendons' length are close to the limits, we apply an attractive potential to plane $l_{ij} = L$. In other words, this potential will attract the tendon's length towards the normal length L, which in turn will ensure that mechanical constraint conditions are avoided.

The proposed potential function can be expressed as follows

$$U_{lim}(\mathbf{q}) = \sum_{i=1}^{N}\sum_{j=1}^{3} \sigma(\frac{l_{ij}-L}{\zeta L})^2, \tag{11}$$

where σ is positive constant. The attractive velocity field is as follows

$$\dot{\mathbf{q}}_{lim}(\mathbf{q}) = -2\sigma\frac{1}{\zeta^2 L^2}(\mathbf{l}-\mathbf{L}), \tag{12}$$

where $\mathbf{l} = \begin{bmatrix} l_{11} & \dots & l_{13} & l_{21} & \dots & l_{N3} \end{bmatrix}^T$ and $\mathbf{L} = L\mathbf{1}_{3N\times 1}$.

However, producing a potential field with this behavior will reduce the accuracy of the end effector planning to reach a desired position in workspace. It is caused by the fact that this new added potential will keep the resultant velocity field in the actuator space equals zero although the end effector does not reach the desired target point yet. Thus, we need to define a weight function which will reduce the newly-added potential field's contribution as the end effector approaches the target position as follows

$$w(\mathbf{x}) = (1 - e^{-\mu\|(\mathbf{x}-\mathbf{x}_d)\|}), \tag{13}$$

where μ is positive constant. An illustration of the potential as a function of the tendon's length and the distance between the end effector and the target is shown in Figure 2b. The overall actuator space potential field is added to (9). This potential does not affect the base's movement, $\dot{\mathbf{q}}_0 \in \mathbb{R}^6$, so the total new potential $\dot{\mathbf{q}}_{new}(\mathbf{q}) \in \mathbb{R}^{(3N+6)}$ can be expressed as follows

$$\dot{\mathbf{q}}_{new}(\mathbf{q},\mathbf{x}) = \begin{bmatrix} \mathbf{0}_{6\times 1} \\ w(\mathbf{x})\dot{\mathbf{q}}_{lim}(\mathbf{q}) \end{bmatrix} \tag{14}$$

The total potential field in the actuator space can be expressed as

$$\dot{\mathbf{q}}(\mathbf{q}) = \mathbf{J}_e(\mathbf{q})^+ \dot{\mathbf{x}}_{\mathbf{x}_d}(\mathbf{x}) + \sum_{a=1}^{m}\sum_{b=1}^{n} \mathbf{J}_a(\mathbf{q})^+ \dot{\mathbf{x}}_{\mathscr{O}_b}(\mathbf{x}) + \dot{\mathbf{q}}_{new}(\mathbf{q},\mathbf{x}) \tag{15}$$

IV. SIMULATION RESULTS

The algorithm is implemented in a constant-curvature kinematic model of a continuum manipulator in the Robot Operating System (ROS) Environment. All simulations in this section are run in real-time. The simulation is implemented on a computer platform with an Intel Core i3 @2.40

TABLE I
PROPERTIES OF MANIPULATOR AND POTENTIAL FIELD

Number of segments (N)	3
Total Number of PSPs (m)	9
Number of Obstacles (n)	2
Manipulator's radius (d)	0.0134 m
Attractive Field Constant (k)	5.0 (s) or 0.1 (e)
Repulsive Field Constant (η)	3×10^{-7} (s) or 2×10^{-9} (e)
Limit of Potential Influence (ρ_0)	0.025
Maximum extension ratio (ζ)	0.3
Normal length (L)	0.012 m
Constraint-Potential-Field constant (σ)	0.04167
Weight constant (μ)	2.5

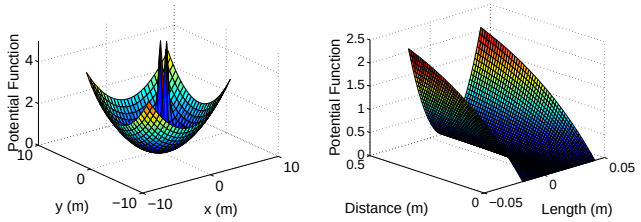

(a) (b)

Fig. 2. (a) Illustration of combined attractive and repulsive potential function applied to a manipulator whose C-Space is in $\mathbb{R}^2$. (b) Illustration of the proposed potential function designed to satisfy mechanical constraint as function of the tendon's length and end-effector-to-target Euclidean distance.

GHz and 1.5 GB RAM running the Linux Mint 13 Operating System.

We use a three-segment manipulator ($N = 3$) with a 6-degree-of-freedoms movable base. We choose 3 PSPs distributed uniformly along the body of each segment. The obstacles are assumed to have a spherical form with a radius equals 0.01 m. The complete properties of the manipulator and the potential field constants, both in simulation (s) and experiment (e) are given in Tab. I.

A. Moving Obstacle with a Static Target

In the first simulation, we simulate two dynamic obstacles moving in a space close to the manipulator. The tip's target position is assumed to be constant. The initial value of actuator space variables are chosen such that the initial position of the end effector coincides with the target. Each obstacle moves in XY-plane with a constant velocity.

From Figure 3, we can see that the manipulator successfully avoids the dynamic obstacles (black spheres) moving close to its body. Besides the repulsive avoid-obstacle movement, the attractive go-to-goal potential is still applied to the end effector of the manipulator, resulting in its movement back to the target point (small red dot) when the obstacle influence disappears after moving farther away from the manipulator's body, as shown in the lower right picture. In Figure 4, the moving obstacle moves in the vicinity of the bottom segment. We can see how the manipulator with its movable base avoids the obstacle while at the same time ensures that the end effector stays on the target position.

The comparison is made in terms of average execution time per cycle between the proposed algorithm and a previous proposed approach [16] employing real-time redundancy-based-obstacle avoidance as shown in Tab. II. Employing the same simulation environment and machine specification, it is shown that the proposed algorithm has an execution time per cycle of 0.2423 s compared to previously proposed redundancy-based planning with an execution time per cycle of 1.1751 s. This is due to the fact that the computational load of the proposed method is lower when compared to the computational load of the previous approach. Hence, the proposed algorithm is relatively more efficient and more suitable for high-speed real-time applications.

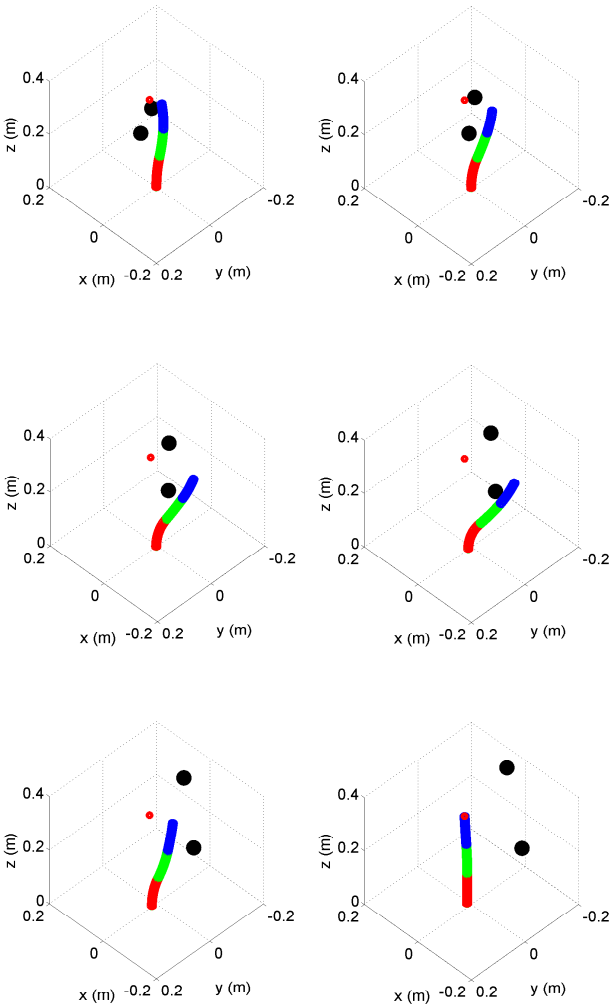

Fig. 3. The movement of the 3-segments-continuum-manipulator with a static target position (small red dot) when 2 obstacles (2 black spheres) move in the vicinity of the manipulator's tip. The order of movement is as follows: upper left picture, upper right picture, lower left picture, and finally lower left picture.

B. Static Obstacle with a Moving Target

In the second simulation, the environment consists of two static obstacles floating in space close to the manipulator's desired trajectory. The tip's target position is assumed to move with a constant velocity ($\|\dot{\mathbf{x}}_d\| = 0.001$ m/s) at each iteration. The velocity vector points from the initial target position to the final target position. The initial value of the tendon length and target position are chosen to have the same value as in the first simulation. The obstacles are located in space close to the target's path.

From Figure 5, we can see that the manipulator starts to track the moving target point (small red dot). When the tendons' length approach the limits, the proposed potential field term $\dot{\mathbf{q}}_{new}(\mathbf{q}, \mathbf{x})$ will be big enough to avoid the tendon increasing its length. This will in turn lead to a motion of the redundant, movable base in the direction of the moving target as a result of the attractive field. Hence, the proposed

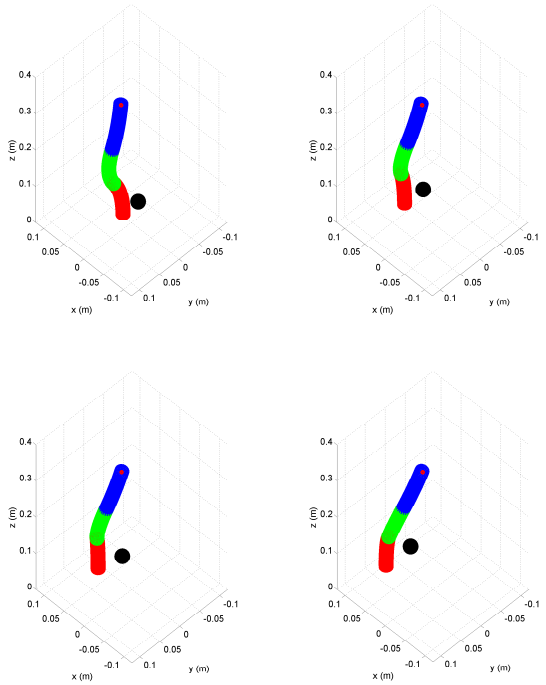

Fig. 4. The movement of the 3-segments-continuum-manipulator with a static target position (small red dot) when moving obstacle (black sphere) move in the vicinity of the manipulator's bottom segment. The order of movement is as follows: upper left picture, upper right picture, lower left picture, and finally lower left picture.

TABLE II
AVERAGE EXECUTION TIME PER CYCLE COMPARISON

Case	Execution Time per Cycle (s)	
	Proposed Algorithm	Redundancy-based Algorithm
A	0.2423	1.1751
B	0.1841	1.1050

potential field enables the manipulator to track the target smoothly and without violating its mechanical constraints. Our mechanical-constraint-potential-field method is superior to standard hard-limiting function used to satisfy the mechanical constraint, since the proposed method does not disturb the smoothness of the movement of the continuum manipulator. Besides that, the manipulator also successfully avoids the obstacles on its path.

As with the previous simulation, in terms of average execution time per cycle shown in Tab. II, the proposed algorithm is more efficient (with an average execution time per cycle of 0.1841 s) than the redundancy-based path planning algorithm in [16] (with an average execution time per cycle of 1.1050 s).

V. EXPERIMENTAL RESULTS

A. System Description

The proposed algorithm is implemented in a tendon-driven single segment continuum manipulator, as presented in [19], as shown in 1a. In this experiment, it is assumed that the

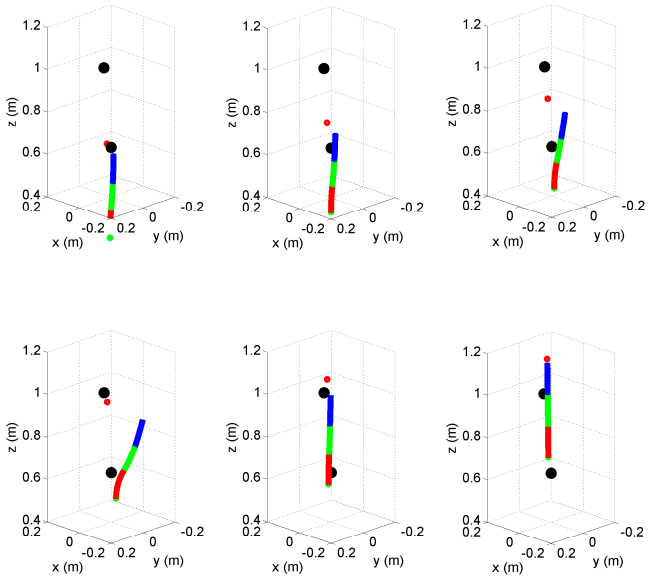

Fig. 5. The movement of the 3-segments-continuum-manipulator with a moving target position (small red dot) and 2 static obstacles (2 black spheres) floating in space close to the manipulator's desired path. The order of movement is as follows: upper left picture, upper right picture, lower left picture, and finally lower left picture.

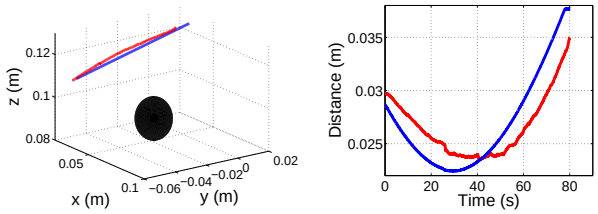

(a) (b)

Fig. 6. (a) The manipulator's tip (red line) tracks the desired trajectory (blue line) and avoids static obstacle (black spheres) nearby. (c) The graph shows the closest distance from the obstacle to the estimated manipulator's body (red line) and to the target (blue line) respectively.

PSP is located only at the tip. The obstacle is assumed to be a point located close to the manipulator's tip.

We use three Maxon DC Motors as actuators. Each motor, equipped with encoders to ensure precise velocity control, is connected to the manipulator's tendons via a gearbox with a 128:1 reduction ratio. The rotational speed of the motors governs the tendons' linear velocities and changes the tendons' lengths.

The end effector position is measured by tracking the electromagnetic-based Aurora sensor coil embedded in the tip of the manipulator. The second sensor coil is hung in the air by a thread to represent the center of the static spherical obstacle with a radius of 0.01 m. The information is fed to the computer via the NDI Aurora tracking system. The target's trajectory is chosen to be a straight line measured with respect to the base of the robot.

B. Results and Discussion

In Figure 6a, the target's movement is drawn with a blue line, the tip's movement is drawn with a red line, and the obstacle is drawn as black spheres. The tip's manipulator starts to track the desired trajectory because of the attractive field induced by the target. The repulsive movement occurs when a part of the manipulator's body enters the region of the obstacle's influence so that the tip's movement deviates from the desired path away from the obstacle.

Figure 6b shows the closest Euclidean distance from the obstacle to the estimated manipulator's body (drawn with a red line) and to the target (drawn with a blue line) respectively. We can observe that when the distance between the obstacle and the tip is less than $\rho_0 = 0.025$ m (i.e. the limit distance of obstacle's influence), the tip does not monotonically follow the target, but instead keeps a certain distance from the obstacle until the moment when the distance between target and obstacle is greater than ρ_0. This confirms that the obstacle-avoidance movement works well for the continuum manipulator prototype in real-time.

One important thing to be noted is that the experiment does not yet guarantee the whole body of the manipulator to be safe from colliding just like in the simulation section. It is due to the fact that the Aurora tracker sensor is only located at the tip.

VI. CONCLUSIONS AND FUTURE WORKS

We propose a potential-field-based real-time path planning algorithm for a multi-segment continuum manipulator. The continuum manipulator's constant-curvature kinematic model is used to test the algorithm. The manipulator moves in space under the influence of artificial potential fields. We also propose a novel potential field in actuator space to satisfy mechanical limits of the manipulator. The overall strategy is tested and verified in a real-time simulator for a 3-segment continuum manipulator and a test is successfully conducted for a tendon-driven single-segment continuum manipulator prototype. The path planning algorithm shows promising result and can be further implemented for real-time planning of other continuum manipulators.

In the future, the algorithm can be equipped with a non-linear observer used to estimate the actuator space variables of the manipulator so that the position of the PSP along the backbone of manipulator can be estimated. This will reduce the risk of collisions between the robot and obstacles. It can also be combined with priori global information of the environment to solve local minima problems.

REFERENCES

[1] W. McMahan, V. Chitrakaran, M. Csencsits, D. Dawson, I. Walker, B. Jones, M. Pritts, D. Dienno, M. Grissom, and C. Rahn, "Field trials and testing of the OctArm continuum manipulator," in *Robotics and Automation, 2006. ICRA 2006. Proceedings 2006 IEEE International Conference on*, May 2006, pp. 2336–2341.

[2] S. Hirose, *Biologically inspired robots: snake-like locomotors and manipulators*, ser. Oxford science publications. Oxford University Press, 1993. [Online]. Available: https://books.google.co.uk/books?id=TaIQAQAAMAAJ

[3] Y.-J. Kim, S. Cheng, S. Kim, and K. Iagnemma, "A Novel Layer Jamming Mechanism With Tunable Stiffness Capability for Minimally Invasive Surgery," *Robotics, IEEE Transactions on*, vol. 29, no. 4, pp. 1031–1042, Aug. 2013.

[4] T. Mahl, A. Hildebrandt, and O. Sawodny, "A Variable Curvature Continuum Kinematics for Kinematic Control of the Bionic Handling Assistant," *Robotics, IEEE Transactions on*, vol. 30, no. 4, pp. 935–949, Aug. 2014.

[5] F. Maghooa, A. Stilli, Y. Noh, K. Althoefer, and H. Wurdemann, "Tendon and pressure actuation for a bio-inspired manipulator based on an antagonistic principle," in *Robotics and Automation (ICRA), 2015 IEEE International Conference on*, May 2015, pp. 2556–2561.

[6] R. J. Webster, III and B. A. Jones, "Design and Kinematic Modeling of Constant Curvature Continuum Robots: A Review," *Int. J. Rob. Res.*, vol. 29, no. 13, pp. 1661–1683, Nov. 2010. [Online]. Available: http://dx.doi.org/10.1177/0278364910368147

[7] V. Duindam, J. Xu, R. Alterovitz, S. Sastry, and K. Y. Goldberg, "Three-dimensional Motion Planning Algorithms for Steerable Needles Using Inverse Kinematics," *I. J. Robotic Res.*, vol. 29, no. 7, pp. 789–800, 2010. [Online]. Available: http://dx.doi.org/10.1177/0278364909352202

[8] G. Niu, Z. Zheng, and Q. Gao, "Collision free path planning based on region clipping for aircraft fuel tank inspection robot," in *Robotics and Automation (ICRA), 2014 IEEE International Conference on*, May 2014, pp. 3227–3233.

[9] D. Palmer, S. Cobos-Guzman, and D. Axinte, "Real-time method for tip following navigation of continuum snake arm robots," *Robotics and Autonomous Systems*, vol. 62, no. 10, pp. 1478 – 1485, 2014. [Online]. Available: http://www.sciencedirect.com/science/article/pii/S0921889014001080

[10] L. Lyons, R. Webster, and R. Alterovitz, "Motion planning for active cannulas," in *Intelligent Robots and Systems, 2009. IROS 2009. IEEE/RSJ International Conference on*, Oct. 2009, pp. 801–806.

[11] L. Torres and R. Alterovitz, "Motion planning for concentric tube robots using mechanics-based models," in *Intelligent Robots and Systems (IROS), 2011 IEEE/RSJ International Conference on*, Sep. 2011, pp. 5153–5159.

[12] C. Bergeles and P. Dupont, "Planning stable paths for concentric tube robots," in *Intelligent Robots and Systems (IROS), 2013 IEEE/RSJ International Conference on*, Nov. 2013, pp. 3077–3082.

[13] J. Xu, V. Duindam, R. Alterovitz, and K. Goldberg, "Motion planning for steerable needles in 3d environments with obstacles using rapidly-exploring Random Trees and backchaining," in *Automation Science and Engineering, 2008. CASE 2008. IEEE International Conference on*, Aug. 2008, pp. 41–46.

[14] J. Xiao and R. Vatcha, "Real-time adaptive motion planning for a continuum manipulator," in *Intelligent Robots and Systems (IROS), 2010 IEEE/RSJ International Conference on*, Oct. 2010, pp. 5919–5926.

[15] G. Chen, M. T. Pham, and T. Redarce, "Sensor-based guidance control of a continuum robot for a semi-autonomous colonoscopy," *Robotics and Autonomous Systems*, vol. 57, no. 67, pp. 712 – 722, 2009. [Online]. Available: http://www.sciencedirect.com/science/article/pii/S0921889008002042

[16] I. Godage, D. Branson, E. Guglielmino, and D. Caldwell, "Path planning for multisection continuum arms," in *Mechatronics and Automation (ICMA), 2012 International Conference on*, Aug. 2012, pp. 1208–1213.

[17] O. Khatib, "Real-time obstacle avoidance for manipulators and mobile robots," in *Robotics and Automation. Proceedings. 1985 IEEE International Conference on*, vol. 2, Mar. 1985, pp. 500–505.

[18] S. DiMaio and S. Salcudean, "Needle steering and motion planning in soft tissues," *Biomedical Engineering, IEEE Transactions on*, vol. 52, no. 6, pp. 965–974, Jun. 2005.

[19] P. Qi, C. Qiu, H. Liu, J. Dai, L. Seneviratne, and K. Althoefer, "A novel continuum-style robot with multilayer compliant modules," in *Intelligent Robots and Systems (IROS 2014), 2014 IEEE/RSJ International Conference on*, Sep. 2014, pp. 3175–3180.

[20] B. Siciliano, "Kinematic control of redundant robot manipulators: A tutorial," *Journal of Intelligent and Robotic Systems*, vol. 3, no. 3, pp. 201–212, 1990. [Online]. Available: http://dx.doi.org/10.1007/BF00126069